JSS Focus Issue on Nanocarbons—In Memory of Sir Harry Kroto

Fullerene-Based n-Type Materials That Can Be Processed by a Photoprecursor Approach for Photovoltaic Applications

Kazuki Kawajiri,[a] Takahiro Kawanoue,[a] Masaki Yamato,[b] Kengo Terai,[a] Masataka Yamashita,[a] Mari Furukawa,[a] Naoki Aratani,[a] Mitsuharu Suzuki,[a,z] Ken-ichi Nakayama,[b,c,z] and Hiroko Yamada[a,z]

[a]*Graduate School of Materials Science, Nara Institute of Science and Technology, Ikoma, Nara 630-0192, Japan*
[b]*Department of Organic Device Engineering, Yamagata University, Yonezawa, Yamagata 992-8510, Japan*
[c]*Department of Material and Life Science, Osaka University, Suita, Osaka 565-0871, Japan*

The active layer of organic photovoltaic cells (OPVs) is typically a blend of p- and n-type semiconductors, and the arrangement of these materials largely affects the device performance. We have recently proposed a unique deposition technique in which α-diketone-type photoprecursors are solution-deposited and then subjected to in-situ photoreaction to form acene-based semiconductors, as an effective means for controlling the morphology and vertical composition profile in organic molecular blends. However, the applicability of this "photoprecursor approach" has been limited to *p-type* materials so far, restricting the flexibility in designing photovoltaic layers. Herein, we report α-diketone-type photoprecursors of two fullerene–anthracene conjugates which have been designed to serve as *n-type* material in OPVs. The new α-diketones, named N601DK and N602DK, are successfully applied to the photoprecursor approach, affording smooth thin films of the corresponding photoreaction products N601 and N602. The n-type materials thus produced are evaluated in bulk-heterojunction (BHJ) OPVs and found to show good photovoltaic response. Especially, N601 performs as well as $PC_{61}BM$, a fullerene-based benchmark n-type material. These results will serve as a basis for further improvement of OPVs through optimization of the molecular arrangement in solution-processed photovoltaic layers.

Manuscript submitted December 13, 2016; revised manuscript received January 12, 2017. Published January 25, 2017. *This paper is part of the JSS Focus Issue on Nanocarbons – In Memory of Sir Harry Kroto.*

Fullerenes and their derivatives constitute the most extensively studied class of n-type semiconductors for use in organic photovoltaic cells (OPVs). Especially, a well-soluble methanofullerene derivative [6,6]-phenyl-C_{61}-butyric acid methyl ester ($PC_{61}BM$)[1] and its sibling compound [6,6]-phenyl-C_{71}-butyric acid methyl ester ($PC_{71}BM$)[2] have been considered as the standard n-type materials in solution-processed organic photovoltaic layers. The strength of these compounds lies in the well-balanced electronic and electric properties of fullerene cages and the high processability derived from the flexible addend. Indeed, a large part of the OPV research reported so far, from the study of elementary processes and limiting factors to the optimization of material design and thin-film morphology, has been based on the use of $PC_{61}BM$ or $PC_{71}BM$ as n-type material.[3] As such, although several high-performance nonfullerene n-type materials have been reported recently,[4–8] fullerenes are still attractive scaffolds in constructing new n-type molecules for OPVs,[9–11] if one considers their favorable characteristics and the rich accumulated knowledge.

Meanwhile, we are applying a "photoprecursor approach" to the preparation of organic photovoltaic layers, in which semiconducting thin films are prepared by solution deposition of precursors followed by in-situ photoreaction to generate corresponding target compounds. Specifically, our process employs α-diketone-type photoprecursors that can be quantitatively converted to acene compounds with extrusion of carbon monoxide upon visible-light irradiation (Figure 1a).[12] We have shown that this method is effective in preparing well-performing photovoltaic layers comprising highly crystalline, scarcely soluble p-type molecular semiconductors which are otherwise hard to process by solution-based techniques.[13–15] The photoprecursor approach is also useful for the preparation of multilayer thin films by solution processes, provided that the solubility of photoreaction product is low enough not to be washed away upon the solution deposition of another layer. This enables the control of vertical composition profile in organic photovoltaic layers,[16] which is a critical factor in determining the performance of OPV, without relying on the use of vacuum process, orthogonal solvents, or polymerization-based curing. However, application of the photoprecursor approach has been limited to p-type materials, and to our knowledge there have been no reports on n-type small-molecule semiconductors that can be processed by the photoprecursor approach for photovoltaic applications.

With these in mind, we have launched a project toward achieving high-performance insoluble n-type materials that can be processed by the photoprecursor approach for use in OPVs. Successful preparation of such materials will largely expand the scope in design and control of the active-layer structure; for example, multilayer structures may be constructed by combining such an insoluble n-type material with any of known high-performance solution-processable p-type materials. Note here that the variety of available p-type OPV materials is much wider than that of n-type materials. In addition, it will become possible to prepare inverted multilayer structures in which an n-layer comes at the bottom of photovoltaic layer. Inverted bulk-heterojunction (BHJ) devices are known to be superior to the normal-structure counterparts in terms of device efficiency and stability,[17] which may be also the case for multilayer devices.

This contribution reports the first-generation materials along this line. The target α-diketone-type photoprecursors, named N601DK and N602DK, are designed to quantitatively afford the corresponding fullerene–anthracene conjugates N601 and N602 upon photoirradiation (Figure 1b, 1c). Following sections describe the synthesis and photoreactivity of the target photoprecursors, and electronic properties of the thin films prepared by the photoprecursor approach. Furthermore, the performance of N601 and N602 as n-type material is comparatively examined in BHJ OPVs using poly(3-hexylthiophen-2,5-diyl) (P3HT) as p-type material. It is shown that the relatively small structural difference between N601 and N602 leads to significant change in OPV performance.

Experimental

Materials.—The photoprecursors N601DK and N602DK were synthesized as outlined in Figure 2 and characterized by nuclear magnetic resonance (NMR) spectroscopy, infrared (IR) spectroscopy, and mass (MS) spectrometry. The detailed synthetic procedures and

[z]E-mail: msuzuki@ms.naist.jp; nakayama@ms.eng.osaka-u.ac.jp; hyamada@ms.naist.jp

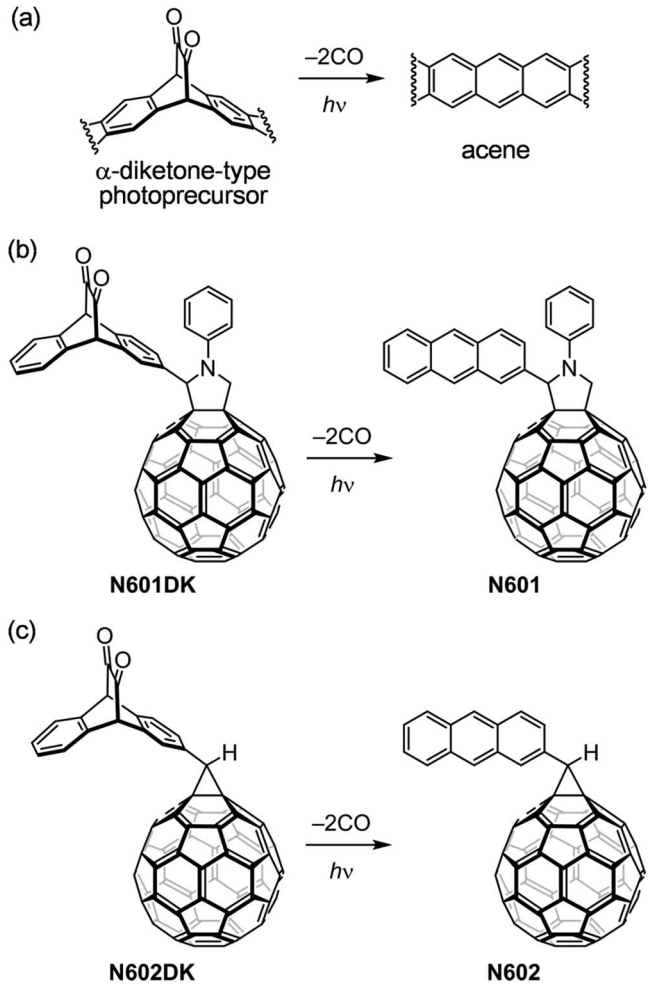

Figure 1. Photoconversion of α-diketone-type precursors to acene derivatives: (a) General scheme; (b) N601DK to N601; and (c) N602DK to N602.

spectroscopic/spectrometric data are reported in Supplementary Material. The purities of N601DK and N602DK were confirmed to be >99% by high-performance liquid chromatography (HPLC) on a reverse-phase column (Inertsil ODS-3, acetonitrile/dichloromethane (1:1)) before use in device fabrication. $PC_{61}BM$ and P3HT were purchased from Luminescence Technology Corp. and used as received. Other reagents and solvents were reagent-grade products purchased from commercial vendors and used without further purification if not specified otherwise in Supplementary Material.

Computation.—All calculations were performed using the Gaussian 09 program suite.[18] Geometry optimizations were performed by density functional theory (DFT) at the B3LYP/6-31G(d) level of theory. Vibrational frequencies were computed for all optimized structures to verify that the obtained structures were minima. The electronic structures were calculated on the optimized geometries by time-dependent DFT (TD-DFT) at the CAM-B3LYP/6-31G+(d) level of theory.

Measurements.—^{1}H NMR measurements for photoreaction monitoring in solution were performed on a JEOL JNM-ECX500 (500 MHz) spectrometer at 298 K. Each sample solution was prepared by dissolving approximately 1 mg of a photoprecursor in 0.5–0.6 ml of chloroform-*d* in an NMR tube equipped with a J. Young valve. After deoxygenated by argon bubbling, the sample was irradiated with a metal-halide lamp (PCS-MH375RC, Nippon P · I) and subjected to ^{1}H NMR measurements every 10 min.

IR spectra of thin films before and after the photoreaction were recorded on a Jasco FT/IR-4200 spectrometer with an RAS PRO410-H attachment. Each sample was prepared on a glass/indium tin oxide (ITO) substrate cleaned by sequential sonication in detergent (Semico Clean 56, Furuuchi Chemical), distilled water, isopropanol (electronics grade, KISHIDA Chemical) for 10 min each followed by UV–O_3 treatment (TC-003, Bioforce Nanoscience) for 30 min. Organic layers were deposited by spin-coating of 10 mg ml^{-1} solutions of N601DK or N602DK in chloroform at a spin rate of 800 rpm for 30 s. The photoirradiation was performed with a blue LED (470 ± 10 nm, 450 mW cm^{-2}, 30 min).

Differential pulse voltammograms (DPVs) were recorded on an ALS electrochemical analyzer Model 612D. The measurements were performed under argon in *o*-dichlorobenzene/benzonitrile (9:1 vol/vol) solutions containing 0.1 M tetra(*n*-butyl)ammonium hexafluorophosphate (n-Bu_4NPF_6) as support electrolyte. The measurement cell consisted of a glassy carbon working electrode, a platinum counter electrode, and a silver/silver nitrate reference electrode. Redox potentials were calibrated with ferrocene/ferrocenium (Fc/Fc^+) redox couple as internal standard.

Electron mobilities were measured by the space-charge-limited-current (SCLC) method using KEITHLEY 2400 SourceMeters operated by LabTracer 2.9 SourceMeter Integration Software. The electron-only devices for the SCLC measurements were prepared as follows: ITO-patterned glass substrates (20 × 20 mm^2) were cleaned by gentle rubbing with an acetone-soaked wipe for about 5 s, sonication in detergent (Semico Clean 56, Furuuchi Chemical) and isopropanol (electronics grade, KISHIDA Chemical) for 10 min each. The washed substrates were further treated in a UV–O_3 cleaner (Bioforce Nanoscience, TC-003) for 30 min. ZnO buffer layers were prepared by a sol–gel method. Zinc acetate (500 mg) was dissolved in a mixture of 2-methoxyethanol (5 mL) and ethanolamine (280 μL), and stirred at 60°C for 12 h. The resulting precursor solution was spin-coated at 4000 rpm for 30 s in air, and thermally annealed at 300°C for 5 min in air. The substrates were then transferred to a N_2-filled grove box (<5 ppm O_2 and H_2O) for preparation of the organic layers. The organic layers were prepared by spin-coating of chloroform solutions of N601DK, N602DK, and $PC_{61}BM$ (14 mg mL^{-1}, 800 rpm, 30 s). For N601DK and N602DK, photoirradiation (LED, 470 ± 10 nm, 400 mW cm^{-2}, 30 min) was performed in the grove box to form corresponding N601 and N602 thin films. Finally, lithium fluoride (1 nm) and aluminum (80 nm) were vapor-deposited at high vacuum (~2 ×10^{-4} Pa) through a shadow mask that defined an active area of 1.0 mm^2.

UV–vis absorption spectra of thin films on glass substrates were recorded in air using a JASCO V-650 spectrometer. Ionization energies were measured on a Bunko Keiki AC-3 photoelectron spectroscopy instrument. The surface morphology of organic films was observed by tapping-mode AFM using an SII SPA400/SPI3800N and a silicon probe with a resonant frequency of 138 kHz and a force constant of 16 N m^{-1} (SII, SI-DF20).

OPV device fabrication and evaluation.—ITO-patterned glass substrates (20 × 25 mm^2, 15 ohm per square) were cleaned by gentle rubbing with an acetone-soaked wipe for about 5 s, sonication in acetone and isopropanol for 10 min each, and exposure to boiling isopropanol for 10 min. The washed substrates were further treated in a UV–O_3 cleaner (Filgen, UV253V8) for 20 min, and poly(3,4-ethylenedioxythiophene):poly(4-styrenesulfonate) (PEDOT:PSS, Clevios P VP AI4083) was spin-coated at 5000 rpm for 40 s in air before a thermal annealing treatment at 120°C for 20 min in air. The thickness of the resulting PEDOT:PSS layer was about 30 nm. The substrates were then transferred to a N_2-filled glove box (<0.5 ppm O_2 and H_2O) for preparation of the organic layers. Finally, calcium (10 nm) and aluminum (80 nm) were vapor deposited at high vacuum (~10^{-5} Pa) through a shadow mask that defined an active area of 4.0 mm^2.

Current-density–voltage (*J*–*V*) curves were measured using a KEITHLEY 2400 source measurement unit under AM1.5G

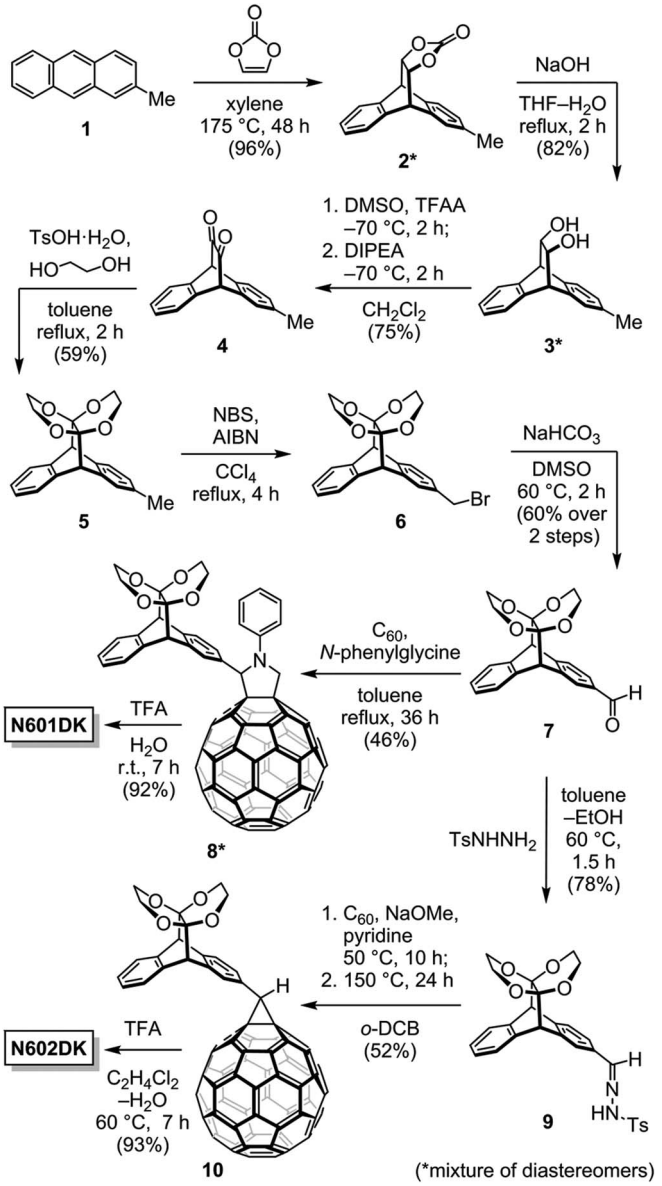

Figure 2. Synthetic routes to the photoprecursors N601DK and N602DK.

illumination at an intensity of 100 mW cm^{-2} using a solar simulator (CEP-2000TF, Bunkoukeiki). The external quantum efficiency (EQE) spectra were obtained under illumination of monochromatic light using the same system. The UV–vis absorption spectra of the organic films including the PEDOT:PSS layer were recorded using a JASCO V-650 spectrophotometer by the transmittance mode.

Results and Discussion

Molecular design and synthesis.—The α-diketone-type photoprecursor of anthracene (ADK) is the photoreactive unit of choice because of the ease in chemical modification and the relatively high reaction quantum yield ($\Phi_r \simeq 0.3$) of the photoinduced decarbonylative aromatization. Larger acenes than anthracene (i.e., tetracene, pentacene, and so on) have been avoided, as their highest occupied molecular orbital (HOMO) levels are too high such that holes are trapped in these acene units hindering efficient hole transport in the p-type material. In addition, introduction of a large addend may hamper efficient contact between fullerene cores and thus electron transport in thin films.

N601 has an *N*-phenylpyrrolidino bridge between the fullerene and ADK units. Introduction of the *N*-phenyl group is in line with the recent report by Karasawa et al. in which structurally related *N*-phenylfulleropyrolidines have been demonstrated as alternatives to $PC_{61}BM$ in BHJ OPVs comprising P3HT or PTB7, a common high-performance polymer,[19] as p-type material. In addition, the relatively high rigidity of the *N*-phenyl moiety was expected to keep the solubility of N601 low enough for enabling the preparation of multilayer structures via the photoprecursor approach. On the other hand, N602 has a methanofullerene-type structure in which the fullerene and ADK units are linked via a single methyne unit. N602 is structurally related to $PC_{61}BM$ in that an aryl group (i.e., phenyl for $PC_{61}BM$ and anthryl for N602) is directly attached on the methano bridge. At the same time, N602 contrasts PCBM in terms of the other substituent on the methano carbon; namely, PCBM is equipped with a butanoic acid methyl ester to ensure the solubility required for solution deposition, while the bridge carbon in N602 is capped with a hydrogen atom. Here again, the latter structural design is in order for keeping the solubility of N602 as low as possible to enable the preparation of multilayer structures in future studies. The solubilities of photoprecursors N601DK and N602DK were expected to be much higher than those of N601 and N602, owing to the high effectiveness of the α-diketone unit as a "solubilizer" as demonstrated in our previous work.[12–16]

Synthetic routes to N601DK and N602DK are summarized in Figure 2. The synthesis was started with the Diels–Alder addition of vinylene carbonate to commercially available 2-methylanthracene (**1**) followed by hydrolysis of the carbonate moiety and Swern oxidation to afford α-diketone derivative **4**. The 11,12-α-diketone unit was then converted to a 11,12;11,12-diethylenedioxy derivative **5** for protection. Here, the reaction conditions were optimized to maximize the selectivity of the 11,12;11,12-diethylenedioxy derivative over the corresponding 11,11;12,12-diethylenedioxy derivative. The methyl group was oxidized to aldehyde by monobromination followed by the dimethyl sulfoxide-mediated oxydation[20] affording the key intermediate **7**.

Aldehyde **7** was reacted with fullerene C_{60} and *N*-phenylglycine to form Prato adduct **8**, which was deprotected to regenerate the α-diketone moiety to give the target photoprecursor N601DK. The other photoprecursor N602DK was obtained in three steps from **7**; dehydration condensation with tosylhydrazide to form hydrazone **9**, addition of **9** to C_{60} under basic conditions to generate adduct **10**, and the deprotection of α-diketone moiety. Note that the reaction between **9** and C_{60} afforded a mixture of [6,6]-close and [5,6]-open adducts, which was converted to pure [6,6]-close adduct by a thermal rearrangement at 150°C. In addition, the deprotection conditions for **10** were slightly modified from those for **8** in order to accommodate the lower solubility of **10** in polar solvents.

Overall, we have successfully established reliable synthetic routes to both of the target photoprecursors, which allow the efficient synthesis and isolation of high-purity materials. In the following experiment, we used the photoprecursors only after confirming that their purities were over 99% by HPLC. It should also be mentioned that the solubilities of N601 and N602 were extremely low, and thus their direct syntheses from 2-formylanthracene were not practical. For example, when we tried the Prato reaction of C_{60} with *N*-phenylglycine and 2-formylanthracene, a complex mixture was obtained as a precipitate which could not be purified because of the low solubility.

Photoreactivity.—The photoreactions of α-diketones N601DK and N602DK to the corresponding anthracene derivatives N601 and N602, respectively, were monitored in solution and in the solid state. The change in ^1H NMR during the photoreactions in chloroform-*d* are shown in Figure 3a, 3b. In both the cases of N601DK and N602DK, the bridgehead protons of α-diketone moieties (H^d, H^e for N601DK and H^j, H^k for N602DK) were decreased and finally disappeared upon photoirradiation. Instead, two additional protons appeared in the aromatic regions corresponding to the formation of anthracene units

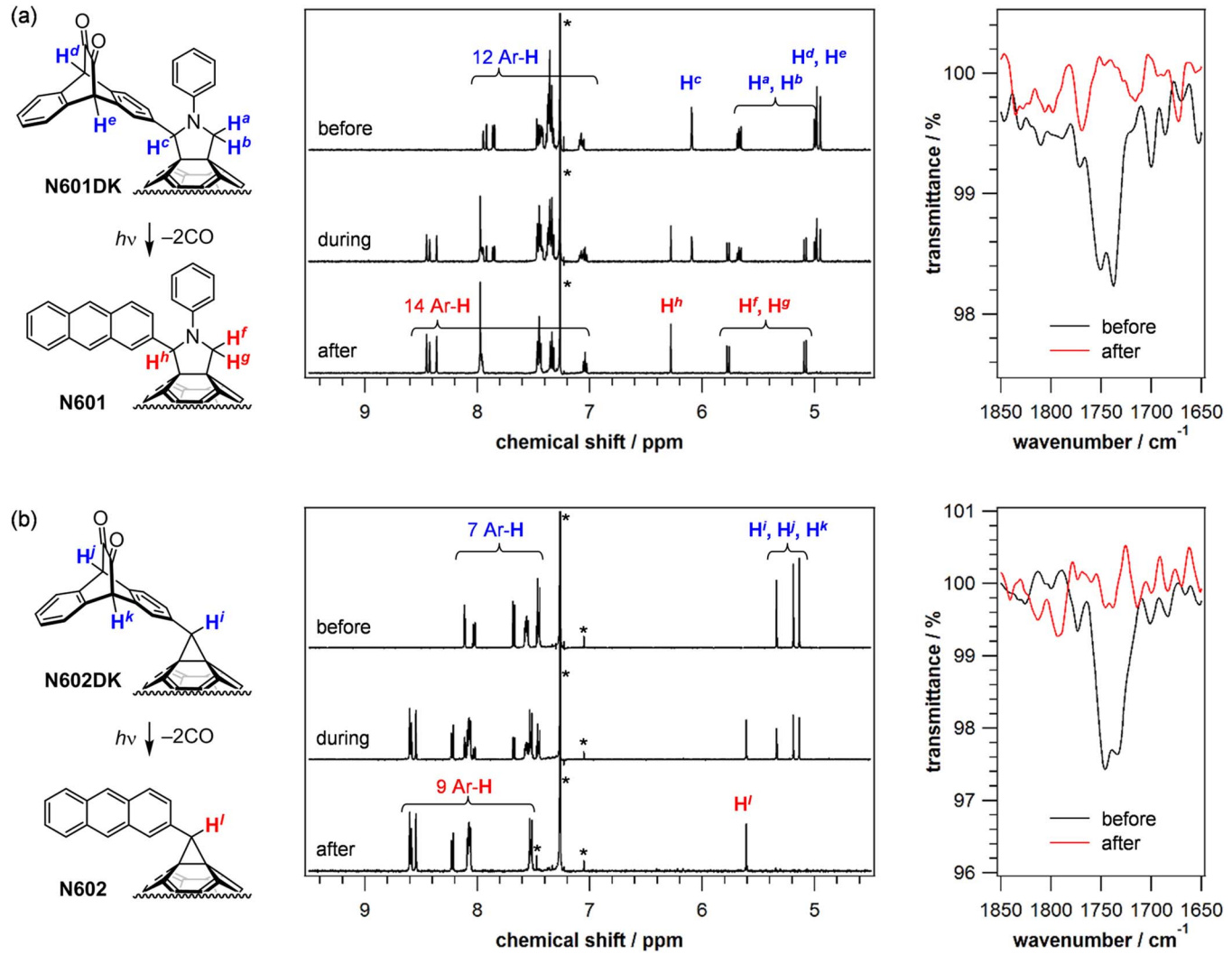

Figure 3. Spectroscopic monitoring of the photoreactions: (a) From N601DK to N601; and (b) From N602DK to N602. (Left) Reaction schemes with the C_{60} cores partially omitted; (Middle) ^{1}H NMR spectra measured in chloroform-*d* before, during, and after the reaction; and (Right) IR spectra of thin films before and after the photoreaction.

by decarbonylative aromatization. This observation indicates quantitative conversion from the α-diketone-type photoprecursors to the anthracene derivatives. Note that the ^{1}H NMR were measured using highly dilute solutions ($\sim 10^{-6}$ M) in order to avoid precipitation of the products during the photoreactions.

The quantitative conversion of α-diketones was confirmed also in the thin-film state by using IR spectroscopy; namely, the carbonyl stretch bands around 1750 cm^{-1} were disappeared after photoirradiation, indicating the complete decarbonylation (Figure 3, right). Additionally, UV–vis absorption of solutions and thin films were measured in which the difference before and after the photoreactions was not significant because the relatively weak absorptions of the α-diketone unit and anthracene moieties are overlapping with the broad absorption of the C_{60} moiety. Nevertheless, the decrease of α-diketone absorption and the appearance of anthracene absorption were detectable, providing further evidence for the successful conversions of N601DK and N602DK to N601 and N602, respectively.

Molecular electronic structures.—The energies of highest-occupied molecular orbitals (HOMOs) and lowest-unoccupied molecular orbitals (LUMOs) of N601 and N602 were determined by differential pulse voltammetry (DPV) following the commonly employed equation, $E_{\mathrm{HOMO/LUMO}} = -(E^{\mathrm{ox/red}} + 4.8)$ eV[21] (Table I and Figure S1 in Supplementary Material). The obtained HOMO levels are –5.41 and –5.52 V for N601 and N602, respectively, being similar to each other but higher than that of $PC_{61}BM$ (–5.77 V). This observation is reasonable because the HOMOs of N601 and N602 are both expected to originate from their anthracene moieties, while the HOMO of $PC_{61}BM$ should be localized at the fullerene core. Note that the HOMO energies of N601 and N602 are well below those of the commonly employed p-type materials (e.g., ca. –5.0 eV for P3HT[22,23] and ca. –5.2 eV for PTB7[19]), and thus the appended anthracene moieties would not act as hole-trapping sites. On the other hand, the LUMO levels are the same for N601, N602, and $PC_{61}BM$ (–3.72 or –3.73 V) indicating that the LUMOs are localized at their fullerene cores and electronically isolated from the addends.

TD-DFT calculations gave essentially the same trend as the experimental observation; namely, the HOMO levels are higher for N601 and N602 as compared to $PC_{61}BM$, while the LUMO levels are very similar within the three compounds (Table I). As expected, these differences and similarities can be explained by the orbital-coefficient distribution (Figure S2 in Supplementary Material). Additionally, the computation results indicate that the slightly higher HOMO level of N601 as compared to N602 is due to the electron donation from the *N*-phenylpyrrolidine unit to the anthracene moiety.

Table I. Comparison of frontier orbital energies and electron mobilities of N601, N602, and $PC_{61}BM$.

compound	$E_{HOMO(DPV)}$[a] [eV]	$E_{LUMO(DPV)}$[a] [eV]	$E_{HOMO(calc)}$[b] [eV]	$E_{LUMO(calc)}$[b] [eV]	$\mu_{e(SCLC)}$ [$cm^2\ V^{-1}\ s^{-1}$]
N601	–5.41	–3.72	–6.87	–2.66	2.6×10^{-4}
N602	–5.52	–3.72	–6.91	–2.64	0.68×10^{-4}
$PC_{61}BM$	–5.77	–3.73	–7.19	–2.62	6.3×10^{-4}

[a]Determined by the redox potentials obtained from DPV measurements and the empirical equation $E_{HOMO/LUMO(DPV)} = -(E^{ox/red} + 4.8)$ eV. $E_{HOMO/LUMO(DPV)}$ values were defined as the onset potentials of the first oxidation/reduction peaks vs. Fc/Fc^+ redox couple.
[b]Calculated at the CAM-B3LYP/6-31G+(d)//B3LYP/6-31G(d) level of theory.

Electron transport in thin films.—Thin films of N601 and N602 were prepared by the photoprecursor approach, and electron mobilities were measured by the SCLC method. Prior to the preparation of electron-only devices for the SCLC measurements, surface morphology of the thin films was observed by tapping-mode atomic force microscopy (AFM) in order for confirming that those films had high enough smoothness and homogeneity to be used in thin-film devices. Note that α-diketone-type photoprecursors usually afford smooth films; however, it has been observed that film morphology significantly changes during the post-deposition photoreaction forming large grains and highly rough surfaces such that the resulting films are inadequate as active layers in organic devices.

The photoprecursor N601DK afforded a smooth surface with a root-mean-square (RMS) roughness of 0.28 nm, and the morphology was not much different after the photoreaction to N601 (Figure 4a, 4b). The film of N602K is also highly smooth, although the RMS roughness (0.66 nm) and apparent grain sizes are slightly larger as compared to the N601DK film. In this case again, surface morphology was not significantly different before and after the photoreaction (Figure 4c, 4d). It should be noted here that the surface roughness of N601DK film is lower than that of $PC_{61}BM$ (RMS roughness = 0.35 nm, Figure S3 in Supplementary Material). This observation demonstrates the capability of the α-diketone unit as inhibitor of extensive self-aggregation to form large grains, being as effective as highly flexible butylic acid methyl ester unit of $PC_{61}BM$. The increased roughness of the N602DK and N602 films compared to the N601DK and N602 films may be ascribed to the reduced size and conformational flexibility of the addends.

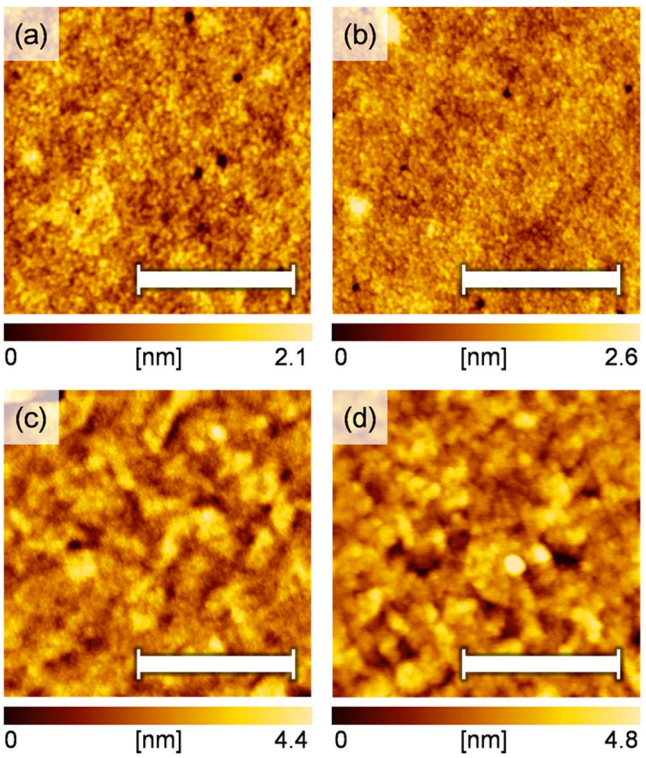

Figure 4. Tapping-mode AFM images of neat films: (a) N601DK (RMS roughness = 0.28 nm); (b) N601 (0.30 nm); (c) N602DK (0.66 nm); and (d) N602 (0.71 nm).The scale bars correspond to 1 μm.

Following the confirmation of the successful preparation of thin films, the electron mobilities in N601 and N602 deposited via the photoprecursor approach were evaluated by the SCLC method. As summarized in Table I, the mobilities are in the order of 10^{-4} to 10^{-5} (see also Figure S4 in Supplementary Material for current-density–voltage curves) which are not very high, yet within the typical values for small-molecule electron-transport materials.[24,25] In comparison with $PC_{61}BM$, the electron mobility in N601 is less than half. Although it is hard to determine a specific reason(s) at this moment, one potential cause for the higher electron mobility in $PC_{61}BM$ would be its smaller addend as compared to N601. The bulkier addend of N601 should more or less keep C_{60} cores from having short contacts and thus forming effective carrier-transport paths in thin films.

On the other hand, the electron mobility in N602 is about four times lower than that in N601, although the smaller addend of N602 has been expected to be advantageous in terms of forming charge-carrier paths as mentioned above. We assume that the lower electron mobility in N602 might be due to the lower homogeneity in film morphology as observed by AFM, which may lead to more frequent occurrence of domain gaps. In relation to this, the morphology and semiconducting performance of thin films prepared by the photoprecursor approach are often largely dependent on the conditions of photoreaction.[13,26] Thus, optimization of the photoreaction conditions (e.g., light intensity, temperature, amount of residual solvent, etc.) may lead to improvement in electron mobility in N601 and N602 as well, which will be reported elsewhere.

Photovoltaic performance.—The final task in this report is to examine if N601 and N602 deposited by the photoprecursor approach can actually serve as n-type materials in OPVs. The evaluation was performed in BHJ devices with the standard p-type polymer P3HT as a partner of N601 and N602. The method and conditions for active-layer deposition were adopted from the literature.[27] The p:n ratio in active layer was fixed at 1:1 by weight in this evaluation, because N601 and N602 worked best in this ratio in a preliminary rough screening where p:n ratios of 2:1, 1:1, and 1:2 were compared.

The obtained photovoltaic parameters are summarized in Table II, and the current-density–voltage (J–V) curves of champion cells are plotted in Figure 5a. Under the examined conditions, N601 afforded higher PCEs than $PC_{61}BM$ (2.43% vs 2.16% in champion cells). The most part of this improvement can be ascribed to the increase in V_{OC} from 0.63 to 0.71 V, which is rather unexpected considering that the LUMO levels of the two materials are essentially the same (Table I). The V_{OC} can be in principle correlated with the energy difference between the HOMO of p-type material and the LUMO of n-type material,[28] and thus it was expected to be similar between the P3HT:N601 and P3HT:$PC_{61}BM$ systems. Interestingly, the V_{OC} of 0.71 V is higher than those observed with the *N*-phenylfulleropyrrolidines examined by Karasawa et al. which showed V_{OC}s of up to 0.65 V when combined with P3HT.[11]

Table II. Photovoltaic parameters of the BHJ OPVs.[a]

n-type material	J_{SC} [mA cm^{-2}]	V_{OC} [V]	FF [%]	PCE [%]
N601	5.47 (5.51 ± 0.13)	0.714 (0.706 ± 0.005)	62.3 (58.2 ± 2.5)	2.43 (2.27 ± 0.13)
N602	4.85 (4.73 ± 0.12)	0.604 (0.595 ± 0.019)	49.0 (48.0 ± 2.3)	1.45 (1.38 ± 0.09)
$PC_{61}BM$	5.72 (5.45 ± 0.16)	0.629 (0.627 ± 0.002)	60.1 (61.2 ± 0.9)	2.16 (2.09 ± 0.05)

[a]Showing the parameters of the champion cell in each case followed by the average of five devices in parentheses.

Accordingly, it is probable that the relatively high V_{OC} obtained with N601 is related to the introduction of the anthracene moiety. It is also worth noting that the P3HT:N601 system afforded the same level of PCEs as those obtained in the BHJ system comprising P3HT and 1,2-diphenylfulleropyrrolidine for which the photovoltaic layers were prepared by direct solution deposition, and the best and average PCEs of 2.41 and 2.07%, respectively, were observed.[11]

In contrast to N601, methanofullerene N602 afforded generally lower efficiencies as compared to $PC_{61}BM$. Specifically, the P3HT:N602 system afforded lower J_{SC} and FF than the P3HT:$PC_{61}BM$ system, while the two systems were similar in V_{OC}. The lower J_{SC} can be partly explained by the smaller thickness and thus lower photoabsorption capability of the active layer. The thinner active layer resulted because the concentration of deposition solution was lower for P3HT:N602DK (15 mg ml^{-1}) than for P3HT:$PC_{61}BM$ (25 mg ml^{-1}). On the other hand, the decrease in FF should be related to the considerably lower electron mobility in N602 as compared to $PC_{61}BM$ (0.68 and 6.3 × 10^{-4} cm^2 V^{-1} s^{-1}, respectively). A lower charge-carrier mobility generally leads to increase in charge-recombination probability and decrease in charge-extraction efficiency, resulting in a lower FF as well as J_{SC}. In line with this, when the active-layer thickness was increased by raising the concentration of deposition solution from 15 to 25 mg ml^{-1}, the P3HT:N602 system afforded even lower photovoltaic efficiencies because of further decrease in J_{SC} and FF (Figure S5 in Supplementary Material). Another potential reason for the lower photovoltaic performance of the P3HT:N602 system is unfavorable film morphology. Indeed, AFM analyses revealed that the P3HT:N602 blend had a rougher surface and contains larger grains as compared to P3HT:N601 blend (Figure 5b, 5c).

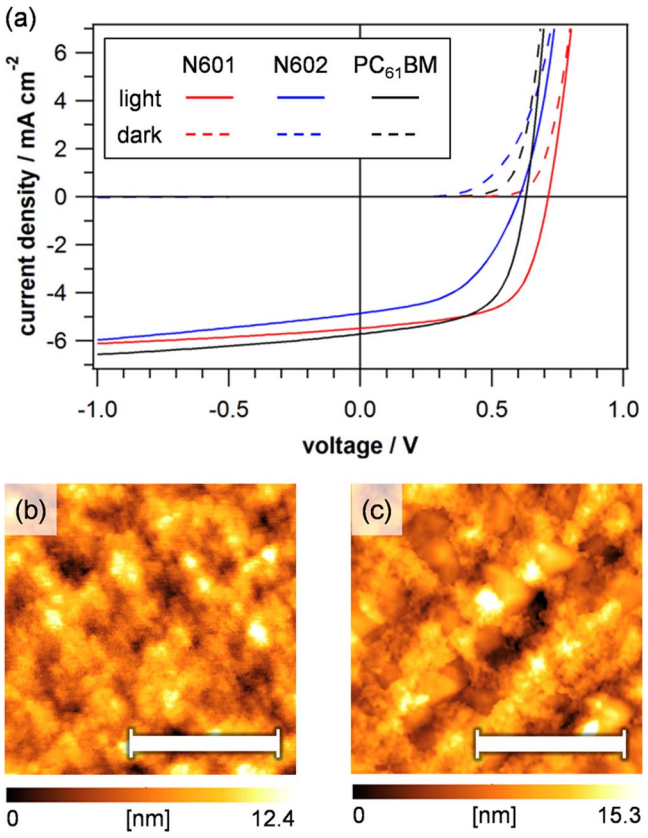

Figure 5. (a) $J-V$ curves (solid lines, under AM1.5G illumination at 100 mW cm^{-2}; dashed lines, in the dark); (b) Tapping-mode AFM images of a P3HT:N601 blend film (RMS roughness = 2.0 nm); (c) Tapping-mode AFM images of a P3HT:N602 blend film (2.5 nm). The scale bars in the AFM images correspond to 1 μm.

Conclusions

This contribution presented α-diketone-type photoprecursors of two fullerene–anthracene conjugates, named N601DK and N602DK, as the first generation of n-type materials that can be processed via the photoprecursor approach for use in OPVs. The photoprecursors were synthesized through an efficient protection–deprotection protocol for the α-diketone moiety, which will be also useful for introducing α-diketone-type photoprecursors of acenes onto various other compounds as a solubility-control subunit. N601DK and N602DK were successfully applied to the photoprecursor approach for preparation of thin films of the corresponding photoreaction products N601 and N602, respectively. The resulting films were highly smooth, and the SCLC measurements showed that the electron mobilities in those films were in the order of 10^{-4}–10^{-5}, being high enough for use in OPVs.

We evaluated their performance in BHJ OPVs using P3HT as p-type material. The *N*-phenylfulleropyrrolidine derivative N601 showed a comparable performance to $PC_{61}BM$, a standard fullerene-based n-type material. On the other hand, the methanofullerene derivative N602 afforded considerably lower PCEs as compared to N601 and $PC_{61}BM$. In addition, the V_{OC} in the P3HT:N601 device was unexpectedly high as compared to the P3HT:N602 and P3HT:$PC_{61}BM$, while N601, N602 and $PC_{61}BM$ show essentially the same reduction potentials in solution. These observations highlight, yet again, the subtle nature of the relationship between molecular structure and solid-state electronic properties of organic small-molecule semiconductors.

Overall this work has successfully demonstrated, for the first time, that the photoprecursor approach can be used for the deposition of fullerene-based n-type materials for OPVs. Note that this method conceptually relates to the precursor approaches reported by Heeger et al. and Imahori et al., where pristine C_{60} is generated in situ via thermally induced retro-Diels–Alder reactions for preparing polymer:C_{60} BHJ layers.[29,30] At the same time, our photoreaction-based approach is distinctive in that the reaction conditions are very mild, requiring in principle only visible-light irradiation. This characteristic allows separating the in-situ chemical reaction and thermal annealing processes, which may enable highly precise morphology tuning upon optimization of processing conditions. We expect that the results obtained herein will greatly promote the applicability of the photoprecursor approach, and paves the way toward the further improvement of solution-processed OPVs through precise control of the active-layer structure.

Acknowledgments

This work was supported by the CREST program of the Japan Science and Technology Agency (JST), Grants-in-Aid for Scientific Research (Nos. 16H02286, 16K17949, 26105004, 25620061,

26288038, and 15H00876 'AnApple'), the program for promoting the enhancement of research universities in NAIST sponsored by the Ministry of Education, Culture, Sports, Science and Technology (MEXT), Japan, Kansai Research Foundation for Technology Promotion (KRF), Grant-in-Aid for the Japan Society for the Promotion of Science (JSPS) Research Fellow (16J04335), and Foundation for NAIST (M. S.). We thank Dr. Yuji Yamaguchi at Yamagata University for helpful discussions.

References

1. G. Yu, J. Gao, J. C. Hummelen, F. Wudl, and A. J. Heeger, *Science*, **270**, 1789 (1995).
2. M. M. Wienk, J. M. Kroon, W. J. H. Verhees, J. Knol, J. C. Hummelen, P. A. van Hal, and R. A. J. Janssen, *Angew. Chem. Int. Ed.*, **42**, 3371 (2003).
3. C. Wang, T. Okabe, G. Long, D. Kuzuhara, Y. Zhao, N. Aratani, H. Yamada, and Q. Zhang, *Dyes Pigments*, **122**, 231 (2015).
4. H. Bin, L. Gao, Z.-G. Zhang, Y. Yang, Y. Zhang, C. Zhang, S. Chen, L. Xue, C. Yang, M. Xiao, and Y. Li, *Nat. Commun.*, **7**, 13651 (2016).
5. S. Holliday, R. S. Ashraf, A. Wadsworth, D. Baran, S. A. Yousaf, C. B. Nielsen, C.-H. Tan, S. D. Dimitrov, Z. Shang, N. Gasparini, M. Alamoudi, F. Laquai, C. J. Brabec, A. Salleo, J. R. Durrant, and I. McCulloch, *Nat. Commun.*, **7**, 11585 (2016).
6. F. Fernández-Lázaro, N. Zink-Lorre, and Á. Sastre-Santos, *J. Mater. Chem. A*, **4**, 9336 (2016).
7. C. B. Nielsen, S. Holliday, H.-Y. Chen, S. J. Cryer, and I. McCulloch, *Acc. Chem. Res.*, **48**, 2803 (2015).
8. W. Chen, X. Yang, G. Long, X. Wan, Y. Chen, and Q. Zhang, *J. Mater. Chem. C*, **3**, 4698 (2015).
9. W. Chen, Q. Zhang, T. Salim, S. A. Ekahana, X. Wan, T. C. Sum, Y. M. Lam, and Alfred H. H. Cheng, Y. Chen, and Q. Zhang, *Tetrahedron*, **70**, 6217 (2014).
10. W. Chen, T. Salim, H. Fan, L. James, Y. M. Lam, and Q. Zhang, *RSC Adv.*, **4**, 25291 (2014).
11. M. Karakawa, T. Nagai, K. Adachi, Y. Ie, and Y. Aso, *J. Mater. Chem. A*, **2**, 20889 (2014).
12. M. Suzuki, T. Aotake, Y. Yamaguchi, N. Noguchi, H. Nakano, K. Nakayama, and H. Yamada, *J. Photochem. Photobiol. C Photochem. Rev.*, **18**, 50 (2014).
13. M. Suzuki, Y. Yamaguchi, K. Takahashi, K. Takahira, T. Koganezawa, S. Masuo, K. Nakayama, and H. Yamada, *ACS Appl. Mater. Interfaces*, **8**, 8644 (2016).
14. C. Quinton, M. Suzuki, Y. Kaneshige, Y. Tatenaka, C. Katagiri, Y. Yamaguchi, D. Kuzuhara, N. Aratani, K. Nakayama, and H. Yamada, *J. Mater. Chem. C*, **3**, 5995 (2015).
15. H. Yamada, Y. Yamaguchi, R. Katoh, T. Motoyama, T. Aotake, D. Kuzuhara, M. Suzuki, T. Okujima, H. Uno, N. Aratani, and K. Nakayama, *Chem. Commun.*, **49**, 11638 (2013).
16. Y. Yamaguchi, M. Suzuki, T. Motoyama, S. Sugii, C. Katagiri, K. Takahira, S. Ikeda, and H. Yamada, *Sci. Rep.*, **4**, 7151 (2014).
17. K. Wang, C. Liu, T. Meng, C. Yi, and X. Gong, *Chem. Soc. Rev.*, **45**, 2937 (2016).
18. *Gaussian 09, Revision E.01. See Supplementary Material for the full citation of Gaussian 09*.
19. Y. Liang, Z. Xu, J. Xia, S.-T. Tsai, Y. Wu, G. Li, C. Ray, and L. Yu, *Adv. Mater.*, **22**, E135 (2010).
20. H. Nace and J. Monagle, *J. Org. Chem.*, **24**, 1792 (1959).
21. Y. Zhou, L. Ding, K. Shi, Y.-Z. Dai, N. Ai, J. Wang, and J. Pei, *Adv. Mater.*, **24**, 957 (2012).
22. B. Burkhart, P. P. Khlyabich, T. Cakir Canak, T. W. LaJoie, and B. C. Thompson, *Macromolecules*, **44**, 1242 (2011).
23. J. Hou, Z. Tan, Y. Yan, Y. He, C. Yang, and Y. Li, *J. Am. Chem. Soc.*, **128**, 4911 (2006).
24. H.-K. Lin, Y.-W. Su, H.-C. Chen, Y.-J. Huang, and K.-H. Wei, *ACS Appl. Mater. Interfaces*, **8**, 24603 (2016).
25. C.-H. Shih, P. Rajamalli, C.-A. Wu, W.-T. Hsieh, and C.-H. Cheng, *ACS Appl. Mater. Interfaces*, **7**, 10466 (2015).
26. K. Nakayama, C. Ohashi, Y. Oikawa, T. Motoyama, and H. Yamada, *J. Mater. Chem. C*, **1**, 6244 (2013).
27. M. T. Dang, L. Hirsch, and G. Wantz, *Adv. Mater.*, **23**, 3597 (2011).
28. M. C. Scharber, D. Mühlbacher, M. Koppe, P. Denk, C. Waldauf, A. J. Heeger, and C. J. Brabec, *Adv. Mater.*, **18**, 789 (2006).
29. T. Umeyama, S. Shibata, and H. Imahori, *RSC Adv.*, **6**, 83758 (2016).
30. J. K. Lee, Y.-M. Wang, S. Cho, F. Wudl, and A. J. Heeger, *Org. Electron.*, **10**, 1223 (2009).